



MCML — Monte Carlo modeling of light transport in multi-layered tissues

Lihong Wang^{*a}, Steven L. Jacques^a, Liqiong Zheng^b

^a*Laser Biology Research Laboratory, Box 17, University of Texas M.D. Anderson Cancer Center, 1515 Holcombe Boulevard, Houston, TX 77030, USA*

^b*Department of Computer Science, University of Houston, Houston, TX 77204-3475, USA*

Received 1 February 1995; revision received 11 April 1995; accepted 26 April 1995

Abstract

A Monte Carlo model of steady-state light transport in multi-layered tissues (MCML) has been coded in ANSI Standard C; therefore, the program can be used on various computers. Dynamic data allocation is used for MCML, hence the number of tissue layers and grid elements of the grid system can be varied by users at run time. The coordinates of the simulated data for each grid element in the radial and angular directions are optimized. Some of the MCML computational results have been verified with those of other theories or other investigators. The program, including the source code, has been in the public domain since 1992.

Keywords: Monte Carlo; Photon transport; Tissue optics; Standard C; Dynamic allocation

1. Introduction

Since Wilson and Adam [1] first introduced Monte Carlo simulations into the field of laser-tissue interactions, it has been widely used to simulate light transport in tissues for various applications and gone through several improvements. [2–7]. Although multiple research groups have implemented Monte Carlo simulations in various computer languages, our Standard C implementation of Monte Carlo modeling of photon transport in multi-layered tissues (MCML), upon which a

light beam is normally incident, is the first one that is portable to multiple computer platforms. We also optimize the coordinates of the scored physical quantities in each grid element, and allocate arrays and matrices dynamically so that the number of tissue layers and grid elements can be varied at run time.

Monte Carlo simulation has been used to solve various physical problems besides laser-tissue interactions. However, there is no distinct and well established definition. We would like to adopt the definition by Lux et al. [8]: ‘In all applications of the Monte Carlo method, a stochastic model is constructed in which the expected value of a certain random variable (or of a combination of

^{*} Corresponding author, Tel.: (713) 792-3664; Fax: (713) 792-3995. Email: lihong@laser.mda.uth.tmc.edu.

several variables) is equivalent to the value of a physical quantity to be determined. This expected value is then estimated by the average of multiple independent samples representing the random variable introduced above. For the construction of the series of independent samples, random numbers following the distribution of the variable to be estimated are used.'

Monte Carlo simulations offer a flexible, yet rigorous approach to photon transport in turbid tissues, which can score multiple physical quantities simultaneously. The method describes local rules of photon propagation that are expressed, in the simplest case, as probability distributions that describe the step size of photon movement between sites of photon-tissue interaction, and the angles of deflection in a photon's trajectory when a scattering event occurs. However, the method is statistical in nature and as such, relies on calculating the propagation of a large number of photons (e.g. 100 000) by the computer. As a result, this method requires a large amount of computational time.

The Monte Carlo simulations are based on macroscopic optical properties that are assumed to extend uniformly over small units of tissue volume. Mean free paths between photon-tissue interaction sites typically range from 10–1000 μm , and 100 μm is a typical value in the visible spectrum [9]. For example, the simulations do not treat the details of radiant energy distribution within cells. The photons are treated as classical particles, and the polarization and wave phenomenon are neglected. The current version does not consider anisotropic media, although the scattering can be anisotropic.

The Monte Carlo simulations may be used for both diagnostic and therapeutic applications of lasers and other optical sources in medicine. For example, Monte Carlo-simulated diffuse reflectance can be used to deduce optical properties of tissues, which may be used to differentiate cancerous tissue from normal tissue. Monte Carlo simulated optical energy deposition inside tissue may be used to compute light dosage for photodynamic therapy of disease.

In the following sections, we will describe the problem we are trying to solve (Section 2), describe how to trace photons in tissues (Section 3) and

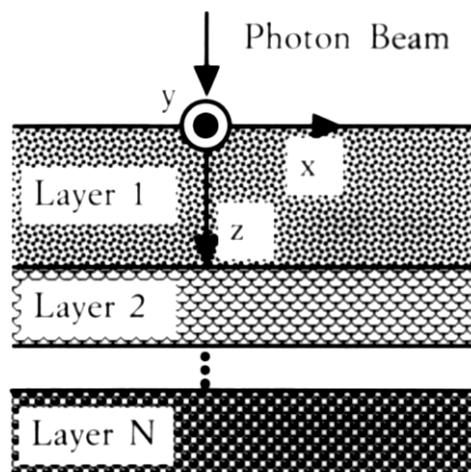


Fig. 1. A schematic of the Cartesian coordinate system set up on multi-layered tissues. The y -axis points outward.

score physical quantities (Section 4), and will present a few MCML computational results (Section 5) followed by a section for conclusions (Section 6).

2. The problem and coordinate systems

The Monte Carlo simulation described in this paper deals with the transport of an infinitely narrow photon beam, perpendicularly incident on a multi-layered tissue (Fig. 1). The responses to the infinitely narrow photon beam are called impulse responses. Each layer is infinitely wide, and is described by the following parameters: the thickness, the refractive index, the absorption coefficient μ_a (cm^{-1}), the scattering coefficient μ_s (cm^{-1}), and the anisotropy factor g . The refractive indices of the ambient medium above the tissue (e.g. air) and the ambient medium below the tissue (if existing) need to be given as well. Although the real tissue can never be infinitely wide, it can be so treated on the condition that it is much wider than the spatial extent of the photon distribution. The tissue layers are parallel to each other.

The absorption coefficient μ_a is defined as the probability of photon absorption per unit infinitesimal pathlength, and the scattering coefficient is defined as the probability of photon

scattering per unit infinitesimal pathlength. For the simplicity of notation, the total interaction coefficient μ_t , which is the sum of the absorption coefficient μ_a and the scattering coefficient μ_s , is sometimes used. Consequently, the interaction coefficient means the probability of photon interaction per unit infinitesimal pathlength. The anisotropy g is the average of the cosine value of the deflection angle [10].

Three coordinate systems are used in the Monte Carlo simulation at the same time. A Cartesian coordinate system is used to trace photon movements. The origin of the coordinate system is the photon incident point on the tissue surface; the z -axis is the normal of the surface pointing toward the inside of the tissue; and the xy -plane is therefore on the tissue surface (Fig. 1).

Since the infinitely narrow photon beam is perpendicular to the tissue surface of a multi-layered tissue, the problem has cylindrical symmetry. Therefore, we set up a cylindrical coordinate system to score internal photon absorption as a function of r and z , where r and z are the radial and z coordinates of the cylindrical coordinate system, respectively. The cylindrical coordinate system and Cartesian coordinate system share the origin and z -axis. The r coordinate of the cylindrical coordinate system is also used for the diffuse reflectance and diffuse transmittance as a function of r and α , where α is the angle between the photon exiting direction and the normal to the tissue surfaces ($-z$ axis for reflectance and z axis for transmittance).

A moving spherical coordinate system, whose z axis is dynamically aligned with the photon propagation direction, is used for sampling of the propagation direction change of a photon packet. In this spherical coordinate system, the deflection angle θ and the azimuthal angle ψ due to scattering are first sampled. Then, the photon direction is updated in terms of the directional cosines in the Cartesian coordinate system (see Section 3.7).

To score physical quantities in the Monte Carlo simulation, we need to set up grid systems. For scoring photon absorption, a two-dimensional homogeneous grid system is set up in the r and z directions. The grid separations are Δr and Δz in the r and z directions, respectively. The total

numbers of grid elements in the r and z directions are N_r and N_z , respectively. For scoring diffuse reflectance and transmittance, a two-dimensional homogeneous grid system is set up in the r and α directions. This grid system can share the r direction with the grid system for photon absorption; therefore, we need to set up one extra one-dimensional grid system for the diffuse reflectance and transmittance in the α direction. The total number of grid elements is N_α . Since we always chose the range of α to be $0 \leq \alpha \leq \pi/2$, the grid separation is $\Delta\alpha = \pi/(2 N_\alpha)$.

Photon absorption, fluence, reflectance, and transmittance are the physical quantities to be simulated. The simulation propagates photons in three dimensions, records photon deposition, $A(r, z)$, in the neighborhood of (r, z) , and converts it into probability of a photon being absorbed per unit volume (cm^{-3}) at the end of tracing multiple photons. The photon probability fluence (cm^{-2}), $\phi(r, z)$, which is the photon probability flow per unit area, can be computed through $A(r, z)$. During the simulation, the absorption or fluence due to the first photon-tissue interactions are singled out and scored separately because they always happen on the z -axis [11]. The simulation also records the escape of photons at the top and bottom surface as reflectance, $R_d(r, \alpha)$, and transmittance, $T_d(r, \alpha)$ ($\text{cm}^{-2}\text{sr}^{-1}$), which is defined as the probability of a photon escaping per unit area at r per unit solid angle around α . Similar to the absorption, the unscattered reflectance or transmittance are scored separately. Physical quantities of lower dimensions can be computed through higher dimensions. For example, photon absorption as a function of z , $A(z)$, can be obtained by integrating $A(r, z)$ over r .

In MCML, for consistency we use centimeter (cm) as the basic unit of length throughout the simulation. For example, the thickness of each layer and the grid separations in the r and z directions are in cm. The absorption coefficient and scattering coefficient are in cm^{-1} .

In some of the discussions, the arrays will simply be referenced by the location of the grid element, e.g. (r, z) or (r, α) , rather than by the indices of the grid element, although the indices are used in the program to reference array elements.

3. Simulating photon propagation

This section presents the rules that define photon propagation in the Monte Carlo model as applied to multi-layered tissues. Some treatment is based upon Ref. 2, which deals with a semi-infinite tissue. We consider multi-layered tissues, and our approach is general enough to include clear media (e.g. glass slides or water layers) as a special case. Fig. 2 shows the basic flowchart for the photon tracing part of the Monte Carlo calculation, which has been implemented in ANSI Standard C. Many boxes in the flowchart are direct implementations of the following discussions.

3.1. Sampling random variables

The Monte Carlo method relies on the random sampling of variables from probability distributions. Several books [8, 12, 13] provide good reference for the principles of Monte Carlo modeling.

For random variable χ , there is a probability density function $p(\chi)$ that defines the distribution of χ over the interval (a, b) . This variable may be the variable step size that a photon will take between photon-tissue interaction sites, or the angle of deflection that a scattered photon may experience due to a scattering event.

To simulate propagation, we want to be able to choose a value for χ repeatedly and randomly based on a pseudo-random number generator provided by a computer. The computer generates a random variable, ξ , which is uniformly distributed over the interval $(0, 1)$. The generally non-uniform probability density function $p(\chi)$ can be sampled by solving the following equation for χ : [8,7,12–14]

$$\int_a^x p(\chi) d\chi = \xi \text{ for } \xi \in (0,1) \quad (3.1)$$

In the following sections, Eq. 3.1 will be repeatedly invoked for sampling propagation variables.

3.2. Representation of a photon packet

Data structures are an important part of the program. Logically related parameters are organized by structures in C such that the program

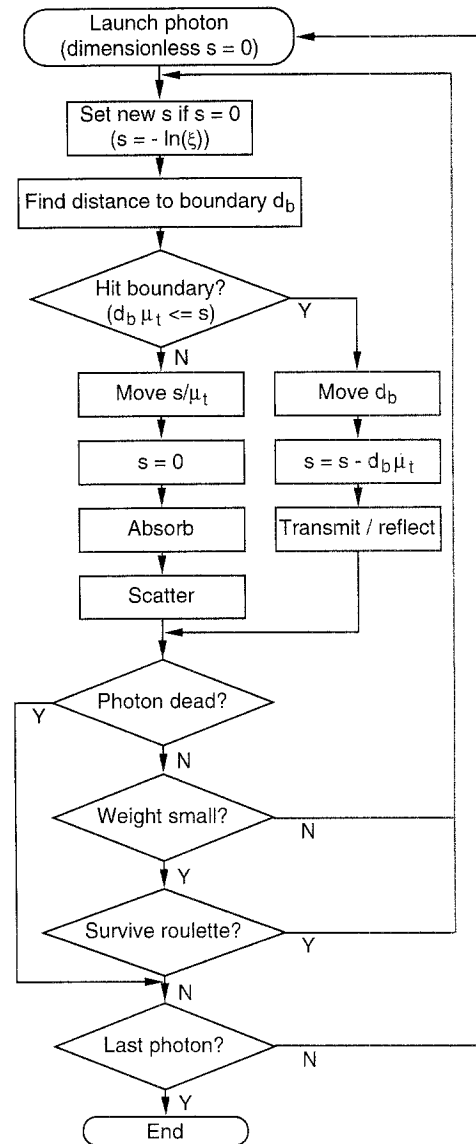


Fig. 2. Flowchart for tracing photons in multi-layered tissues with the Monte Carlo simulation.

is easier to write, read, maintain and modify. The parameters for a photon packet are grouped into a single structure defined by:

```

typedef struct {
    double x, y, z; /* Cartesian coordinates [cm] */
    double ux, uy, uz; /* directional cosines of a photon direction. */
    double w; /* weight. */
    Boolean dead; /* 0/1 if photon is propagating/terminated. */
    double s; /* dimensionless step size to be taken. */
    long scatters; /* number of scatterings. */
    short layer; /* index to layer where photon packet resides. */
} PhotonStruct;
  
```

The location of a photon packet described by the Cartesian coordinates (x, y, z) is represented by the structure members x, y, z . The traveling direction of a photon packet described by the directional cosines (μ_x, μ_y, μ_z) is represented by the structure members ux, uy, uz .

A simple variance reduction technique, implicit photon capture [15], is used to improve the efficiency of the Monte Carlo simulation. This technique allows one to equivalently propagate many photons as a packet along a particular pathway simultaneously. Each photon packet is initially assigned a weight, W , equal to unity. The current weight of the photon packet is denoted by the structure member w .

The member *dead*, initialized to be 0 when the photon packet is launched, represents the status of a photon packet. If the photon packet has exited the tissue or has not survived a Russian roulette (to be discussed) when its weight is below the threshold weight, the member *dead* is set to 1. It is used to signal the program to stop tracing the current photon packet. The type Boolean is not an internal data type in ANSI Standard C, and is defined to be type char in the header file of MCML.

The member *s* is the step size in dimensionless unit, which is also called 'optical distance' and defined as the integration of the interaction coefficient μ_t over the photon pathway. [16] In a homogeneous medium, the optical distance is simply the photon pathlength multiplied by the interaction coefficient. The member *scatters* is used to store the number of scatterings experienced by a photon packet. When photon weight is scored, the member *scatters* is used to identify the unscattered reflectance or transmittance, or the first interactions inside the tissue.

The member *layer* is the index to the layer where the photon packet resides. It is defined for computation efficiency, although the layer can always be identified according to the z coordinate of the photon packet and the geometric structure of the media. The member *layer* is updated only when the photon packet crosses layer interfaces.

3.3. Photon launching

The photon is injected orthogonally onto the tis-

sue at the origin, which corresponds to a collimated infinitely narrow beam of photons. The photon position (x, y, z) is initialized to $(0, 0, 0)$, and the directional cosines (μ_x, μ_y, μ_z) are set to $(0, 0, 1)$. The weight is initialized to 1, and several other structure members including *dead*, *scatters*, and *layer* in the structure PhotonStruct are also initialized.

When the photon is launched, if there is a refractive-index-mismatched interface between the tissue and the ambient medium, then some specular reflectance will occur. If the refractive indices of the outside medium and tissue are n_1 and n_2 , respectively, then the specular reflectance, R_{sp} , is specified: [17, 18]

$$R_{sp} = \frac{(n_1 - n_2)^2}{(n_1 + n_2)^2} \quad (3.2)$$

If the first layer is clear medium, which is on top of a layer of medium whose refractive index is n_3 , multiple reflections and transmissions on the two boundaries of the clear layer are considered. The specular reflectance is then computed by:

$$R_{sp} = r_1 + \frac{(1 - r_1)^2 r_2}{1 - r_1 r_2} \quad (3.3)$$

where r_1 and r_2 are the Fresnel reflectances on the two boundaries of the clear layer:

$$r_1 = \frac{(n_1 - n_2)^2}{(n_1 + n_2)^2} \quad (3.4)$$

$$r_2 = \frac{(n_3 - n_2)^2}{(n_3 + n_2)^2} \quad (3.5)$$

The photon weight, initialized to 1, is decreased by R_{sp} for the photon packet to enter the medium:

$$W = 1 - R_{sp} \quad (3.6)$$

If Eq. 3.2 is used, the structure member *layer* is set to the first layer. Otherwise, Eq. 3.3 is used, and the structure member *layer* is set to the second layer. If, for any reason, there are multiple consecutive layers of clear media and they cannot be combined into one layer due to mismatch of refractive indices, the photon packet will be laun-

ched into the second layer and start propagation with the Monte Carlo method.

3.4. Photon's step size

The step size of the photon packet is calculated based on a sampling of the probability distribution for the photon's free path s ($0 \leq s < \infty$), which is the step size. We will first consider an infinite turbid medium. According to the definition of interaction coefficient μ_t , the probability of photon-tissue interaction per unit pathlength in the interval $(s', s' + ds')$ is:

$$\mu_t = \frac{-dP\{s \geq s'\}}{P\{s \geq s'\}ds'} \quad (3.7)$$

or

$$d(\ln(P\{s \geq s'\})) = -\mu_t ds' \quad (3.8)$$

where $P\{\}$ gives the probability for the condition inside the $\{\}$ to hold. Eq. 3.8 can be integrated over s' in the range $(0, s_1)$ and can lead to an exponential distribution, where $P\{s \geq 0\} = 1$ is used:

$$P\{s \geq s_1\} = \exp(-\mu_t s_1) \quad (3.9)$$

Eq. 3.9 can be rearranged to yield the cumulative distribution function of free path s :

$$P\{s < s_1\} = 1 - \exp(-\mu_t s_1) \quad (3.10)$$

The probability density function of free path s is:

$$p(s_1) = dP\{s < s_1\}/ds_1 = \mu_t \exp(-\mu_t s_1) \quad (3.11)$$

$p(s_1)$ can be substituted into Eq. 3.1 to yield:

$$s_1 = -\ln(1 - \xi)/\mu_t \quad (3.12)$$

or substituting ξ for $(1 - \xi)$ due to the symmetry of ξ about 0.5:

$$s_1 = -\ln(\xi)/\mu_t, \quad (3.13)$$

Eq. 3.13 is used to sample the step size of a photon movement in an infinite or semi-infinite medium.

A simpler approach to derive Eq. 3.12 is to assign the cumulative distribution function to the uniformly distributed random number ξ .

In multi-layered turbid media, the photon packet may experience free flights over multiple layers of media before an interaction occurs. In this case, the counterpart of Eq. 3.9 becomes:

$$P\{s \geq s_{\text{sum}}\} = \exp\left(-\sum_i \mu_{ti}s_i\right) \quad (3.14)$$

where i is the index to a layer, the symbol μ_{ti} is the interaction coefficient for the i th layer, and s_i is the step size in the i th layer. The total step size s_{sum} is:

$$s_{\text{sum}} = \sum_i s_i \quad (3.15)$$

The summation is over all the layers in which the photon packet has traveled. Eq. 3.14 does not take photon reflection and transmission at boundaries into account because they are processed separately. The sampling equation is obtained by equating Eq. 3.14 to ξ :

$$\sum_i \mu_{ti}s_i = -\ln(\xi) \quad (3.16)$$

As you have seen, Eq. 3.13 is a special case of Eq. 3.16 for a single layer. The sampling can be interpreted as that the total dimensionless step size is $-\ln(\xi)$. Note that flights in clear layers do not contribute to the left-hand side of Eq. 3.16 (or the dimensionless step size) because the interaction coefficient is zero.

Eq. 3.16 will be used for sampling step size in MCML, where dimensionless step size s is initialized to $-\ln(\xi)$. Only when the photon packet has traveled through $-\ln(\xi)$ in dimensionless unit will a photon-tissue interaction occur. Therefore, a photon packet may travel multiple substeps of size s_i to reach an interaction site in the multi-layered tissue. When an interaction occurs, the whole photon packet experiences interaction, via either absorption or scattering.

This sampling method involves computation of a logarithm function, which is time-consuming.

Fast methods can be used to alleviate the logarithmic computation [19–21].

3.5. Photon moving

Once a substep s_i (cm) is determined, the photon is moved in the tissue. The position of the photon packet is updated by:

$$\begin{aligned} x &\leftarrow x + \mu_x s_i \\ y &\leftarrow y + \mu_y s_i \\ z &\leftarrow z + \mu_z s_i \end{aligned} \quad (3.17)$$

where the arrows indicate quantity substitutions. The variables on the left-hand side have the new values, and the variables on the right-hand side have the old values. In a C program, an equal sign is used for this purpose.

3.6. Photon absorption

Once the photon has reached an interaction site, a fraction of the photon weight, ΔW , absorbed by the interaction site must be calculated:

$$\Delta W = (\mu_a / \mu_t) W \quad (3.18)$$

which will be deposited in the local grid element. If the photon packet has not been scattered, the photon weight ΔW is scored into the array for first photon-tissue interactions (to be discussed). Otherwise, the photon weight ΔW is scored into $A(r, z)$ at the local grid element:

$$A(r, z) \leftarrow A(r, z) + \Delta W \quad (3.19)$$

The photon weight has to be updated as well by:

$$W \leftarrow W - \Delta W \quad (3.20)$$

The photon packet with the new weight W will suffer scattering at the interaction site.

3.7. Photon scattering

Once the photon packet has reached an interaction site and its weight decreased, the photon packet with the updated weight is ready to be scattered. There will be a deflection angle, θ ($0 \leq \theta < \pi$), and an azimuthal angle, ψ ($0 < \psi < 2\pi$), to be

sampled statistically. The probability distribution for the cosine of the deflection angle, $\cos \theta$, is described by the scattering function that Henyey and Greenstein [10] originally proposed for galactic scattering:

$$p(\cos \theta) = \frac{1 - g^2}{2(1 + g^2 - 2g \cos \theta)^{3/2}} \quad (3.21)$$

where the anisotropy, g , equals $\langle \cos \theta \rangle$ and has a value between -1 and 1 . A value of 0 indicates isotropic scattering and a value near 1 indicates forward-directed scattering. Jacques et al. [22] determined experimentally that the Henyey-Greenstein function describes single scattering in tissue very well. Values of g range between 0.3 and 0.98 for tissues, but quite often g is ~ 0.9 in the visible spectrum. Applying Eq. 3.1, the choice for $\cos \theta$ can be expressed as a function of the random number, ξ :

$$\cos \theta = \begin{cases} \frac{1}{2g} \left\{ 1 + g^2 - \left[\frac{1 - g^2}{1 - g + 2g\xi} \right]^2 \right\} & \text{if } g \neq 0 \\ 2\xi - 1 & \text{if } g = 0 \end{cases} \quad (3.22)$$

Next, the azimuthal angle, ψ , which is uniformly distributed over the interval 0 to 2π , is sampled:

$$\psi = 2\pi\xi \quad (3.23)$$

Once the deflection and azimuthal angles are chosen, the new direction of the photon packet can be calculated: [12]

$$\begin{aligned} \mu'_x &= \sin \theta (\mu_x \mu_z \cos \psi - \mu_y \sin \psi) / \\ &\quad \sqrt{1 - \mu_z^2} + \mu_x \cos \theta \\ \mu'_y &= \sin \theta (\mu_y \mu_z \cos \psi + \mu_x \sin \psi) / \\ &\quad \sqrt{1 - \mu_z^2} + \mu_y \cos \theta \\ \mu'_z &= -\sin \theta \cos \psi \\ &\quad \sqrt{1 - \mu_z^2} + \mu_z \cos \theta \end{aligned} \quad (3.24)$$

If the photon direction is sufficiently close to the

z-axis (e.g. $|\mu_z| > 0.99999$), then the following formulas should be used:

$$\begin{aligned}\mu'_x &= \sin \theta \cos \psi \\ \mu'_y &= \sin \theta \sin \psi \\ \mu'_z &= \text{SIGN}(\mu_z) \cos \theta\end{aligned}\quad (3.25)$$

where $\text{SIGN}(\mu_z)$ returns 1 when μ_z is positive, and returns -1 when μ_z is negative.

In the sampling of the two angles θ and ψ , and the updating of the directional cosines, trigonometric operations are involved. Because trigonometric operations are computation-intensive, we try to minimize them whenever alternative algebraic operations are possible [14].

3.8. Photon hitting a boundary

During a step of size s (dimensionless), the photon packet may hit a boundary of the current layer, where the boundary may either be an interface between the tissue and the ambient medium or an interface between the current layer of tissue and another layer of tissue. The photon packet can be either internally reflected by the boundary or transmit across the boundary. If the photon packet is reflected back into the same layer or crosses into the next layer of tissue, the photon propagation will continue. If the photon packet escapes the tissue to the ambient medium, it will be observed as reflectance or transmittance depending on which ambient-medium-to-tissue interface the photon packet escapes from. Several steps are involved in the simulation when the photon packet hits a boundary of the current layer.

Step 1, the distance between the current photon location (x, y, z) and the boundary of the current layer in the direction of the photon propagation is computed:

$$d_b = \begin{cases} (z_0 - z)/\mu_z & \text{if } \mu_z < 0 \\ \infty & \text{if } \mu_z = 0 \\ (z_1 - z)/\mu_z & \text{if } \mu_z > 0 \end{cases} \quad (3.26)$$

where z_0 and z_1 are the z coordinates of the upper

and lower boundaries of the current layer (see Fig. 1 for the Cartesian coordinate system). If μ_z is zero, the distance is infinity and represented by DBL_MAX in C [23].

Step 2, we decide whether the step size s (dimensionless) is greater than d_b :

$$d_b \mu_t \leq s \quad (3.27)$$

where μ_t is the total interaction coefficient of the current layer. If the above equation holds, the photon packet will hit the boundary, and we move the photon packet to the boundary and update s by $s - d_b \mu_t$, i.e. $s \leftarrow s - d_b \mu_t$.

If Eq. 3.27 does not hold, the step will fit in the current layer, and we move the photon by s/μ_t to reach an interaction site and update s to zero. Now, the photon must experience absorption and scattering. Then, a new dimensionless step size should be generated using $-\ln(\xi)$ and go back to step 1.

Step 3, if the photon packet hits a boundary, we need to compute the probability of a photon packet being internally reflected, which depends on the angle of incidence, α_i , onto the boundary, where $\alpha_i = 0$ means orthogonal incidence. The value of α_i is calculated:

$$\alpha_i = \cos^{-1}(|\mu_z|) \quad (3.28)$$

Snell's law indicates the relationship between the angle of incidence, α_i , the angle of transmission, α_t , and the refractive indices of the media that the photon is incident from, n_i , and transmitted to n_t :

$$n_i \sin \alpha_i = n_t \sin \alpha_t. \quad (3.29)$$

If α_i is larger than the critical angle (possible only when $n_i > n_t$), which is $\sin^{-1}(n_t/n_i)$, the internal reflectance, $R(\alpha_i)$, is set to 1. Otherwise, $R(\alpha_i)$, is calculated by Fresnel's formulas: [17,18]

$$R(\alpha_i) = \frac{1}{2} \left[\frac{\sin^2(\alpha_i - \alpha_t)}{\sin^2(\alpha_i + \alpha_t)} + \frac{\tan^2(\alpha_i - \alpha_t)}{\tan^2(\alpha_i + \alpha_t)} \right] \quad (3.30)$$

which is an average of the reflectances for the two orthogonal polarization directions, because the

light in the simulation is assumed to have no particular polarization. Similar to Section 3.7, the number of trigonometric operations in Eqs. 3.28–3.30 need to be minimized to increase computational speed.

Step 4, we determine whether the photon is internally reflected or transmitted by generating a random number, ξ , and comparing the random number with the internal reflectance, i.e.:

If $\xi \leq R(\alpha_i)$ then the photon is internally reflected (3.31)

If $\xi > R(\alpha_i)$ then the photon transmits.

If the photon is internally reflected, the photon packet stays on the boundary and its directional cosines (μ_x, μ_y, μ_z) must be updated by reversing the z component:

$$(\mu_x, \mu_y, \mu_z) \leftarrow (\mu_x, \mu_y, -\mu_z) \quad (3.32)$$

Then, go back to step 1.

If the photon packet transmits across the boundary, we have to know whether the photon packet has entered another layer of tissue or the ambient medium. If the photon packet is transmitted to the next layer of tissue, it must continue propagation with an updated direction and step size. The new directional cosines are:

$$\begin{aligned} \mu'_x &= \sin \alpha_i \mu_x / \sin \alpha_t \\ \mu'_y &= \sin \alpha_i \mu_y / \sin \alpha_t \\ \mu'_z &= \text{SIGN}(\mu_z) \cos \alpha_i \end{aligned} \quad (3.33)$$

or employing Snell's law (Eq. 3.29), Eq. 3.33 becomes

$$\begin{aligned} \mu'_x &= \mu_x n_i / n_t \\ \mu'_y &= \mu_y n_i / n_t \\ \mu'_z &= \text{SIGN}(\mu_z) \cos \alpha_t \end{aligned} \quad (3.34)$$

Then, go back to step 1 for the next substep of propagation.

If the photon packet escapes the tissue into the ambient medium, the photon weight is scored into diffuse reflectance or transmittance. If the photon

packet has not been scattered, the photon weight is scored into unscattered reflectance or transmittance depending on where the photon packet escapes (to be discussed). If the photon packet has been scattered at least once, the diffuse reflectance, $R_d(r, \alpha_i)$, or diffuse transmittance, $T_d(r, \alpha_i)$, at the particular grid element (r, α_i) must be incremented by the amount of escaped photon weight, W :

$$\begin{aligned} R_d(r, \alpha_i) &\leftarrow R_d(r, \alpha_i) + W \text{ if } z = 0 \\ T_d(r, \alpha_i) &\leftarrow T_d(r, \alpha_i) + W \text{ if } z = \\ &\text{the bottom of the tissue.} \end{aligned} \quad (3.35)$$

Because the photon has completely escaped, the tracing of this photon packet ends here. A new photon may be launched into the tissue and traced thereafter.

An alternative approach toward modeling the effect on the interface between the tissue and the ambient medium may be selected in MCML. Rather than making the internal reflection of the photon packet an all-or-none event, a partial reflection approach can be used each time a photon packet strikes the surface boundary. A fraction $1 - R(\alpha_i)$ of the current photon weight escapes the tissue and increments the local reflectance or transmittance array, i.e. $R_d(r, \alpha_i) \leftarrow R_d(r, \alpha_i) + W(1 - R(\alpha_i))$, or $T_d(r, \alpha_i) \leftarrow T_d(r, \alpha_i) + W(1 - R(\alpha_i))$, or the same amount of weight is scored into the unscattered reflectance or transmittance. The remainder of the photon weight is reflected, and the photon weight is updated as $W \leftarrow W R(\alpha_i)$, and then the propagation continues. The all-or-none approach is faster, but the partial reflection approach may reduce the variance of the reflectance or transmittance.

Since we have avoided dividing by μ_t in identifying boundary crossing, clear layers, which have zero total interaction coefficient, do not have to be treated separately from general tissues. If the photon packet is in a layer of clear medium, the photon packet is moved to the boundary of the clear layer without altering the remaining dimensionless step size because of its zero interaction coefficient μ_t .

3.9. Photon termination

After a photon packet is launched, it can be terminated naturally by reflection or transmission out of the tissue. For a photon packet still propagating inside the tissue, if the photon weight, W , has been sufficiently decreased after many steps of interaction such that it falls below a threshold value (e.g. $W_{th} = 0.0001$), then further propagation of the photon yields little information unless the interest is in the very late stage of photon propagation. However, proper termination must be executed to ensure conservation of energy (or number of photons) without skewing the distribution of photon deposition. A technique called Russian roulette [24,25] is used to terminate the photon packet when $W \leq W_{th}$. The Russian roulette technique gives the photon packet one chance in m (e.g., $m = 10$) of surviving with a weight of mW . If the photon packet does not survive the Russian roulette, the photon weight is reduced to zero and the photon is terminated, i.e.:

$$W \leftarrow \begin{cases} mW & \text{if } \xi \leq 1/m \\ 0 & \text{if } \xi > 1/m \end{cases} \quad (3.36)$$

where ξ is the uniformly distributed pseudo-random number ($0 \leq \xi \leq 1$). This method conserves energy, yet terminates photons in an unbiased manner. The combination of Russian roulette and splitting, which is contrary to roulette, may be used appropriately to reduce variance [24,25].

4. Scored physical quantities

As mentioned earlier, during the Monte Carlo simulation we record the photon reflectance, transmittance, and absorption. In this section we discuss in detail the process of these physical quantities. Dimensions of some of the quantities are shown in square brackets at the end of their respective formulas.

In MCML, 1-D and 2-D physical quantities are stored in 1-D or 2-D arrays correspondingly. These arrays are dynamically allocated [26] at run time so as to allow users to specify the dimension sizes without recompiling the program and wasting memory, which are the problems of defining static arrays.

The last cells in the r and z directions require special attention. Because photons can propagate beyond the grid system, when the photon weight is recorded into the diffuse reflectance or transmittance array, or absorption array, the physical location may not fit into the grid system. In this case, the last cell in the direction of the overflow is used to collect the photon weight; therefore, the last cells in the r and z directions do not indicate the real value at the corresponding locations. However, the angle α is always within the bound we select, i.e. $0 \leq \alpha \leq \pi/2$, hence precluding a problem in the scoring of angular distributions of diffuse reflectance and transmittance.

4.1. Reflectance and transmittance

When a photon packet is launched, the specular reflectance R_{sp} is computed immediately. The photon weight after the specular reflection is transmitted into the tissue. During the simulation, some photon packets may exit the media; their weights are accordingly scored into the diffuse reflectance or diffuse transmittance depending on where the photon packet exits. These packets are internally represented by two arrays $R_{d-ra}[i_r, i_\alpha]$ and $T_{d-ra}[i_r, i_\alpha]$, respectively, in the program, where i_r and i_α are the indices for r and α which are in the range: $0 \leq i_r \leq N_r - 1$, $0 \leq i_\alpha \leq N_\alpha - 1$ for diffuse reflectance or transmittance. Unscattered photon weight is scored into $R_{d-r}[-1]$ and $T_{d-r}[-1]$. The coordinates for each index are optimized to minimize error [27]:

$$r = \left[(i + 0.5) + \frac{1}{12(i + 0.5)} \right] \Delta r \text{ [cm]} \quad (4.1)$$

$$\alpha = (i + 0.5) \Delta \alpha + c \tan[(i + 0.5)\Delta \alpha] \left[1 - \frac{\Delta \alpha}{2} c \tan \left(\frac{\Delta \alpha}{2} \right) \right] \text{ [rad]} \quad (4.2)$$

After tracing multiple photon packets (N), the raw data $R_{d-ra}[i_r, i_\alpha]$ and $T_{d-ra}[i_r, i_\alpha]$ provide the total photon weight in each grid element in the two-dimensional grid system. To compute the total photon weight in the grid elements in each

direction of the two-dimensional grid system, we sum the 2-D arrays in the other dimension:

$$R_{d-r}[i_r] = \sum_{i_\alpha=0}^{N_\alpha-1} R_{d-r\alpha}[i_r, i_\alpha] \quad (4.3)$$

$$R_{d-\alpha}[i_\alpha] = \sum_{i_r=0}^{N_r-1} R_{d-r\alpha}[i_r, i_\alpha] \quad (4.4)$$

$$T_{d-r}[i_r] = \sum_{i_\alpha=0}^{N_\alpha-1} T_{d-r\alpha}[i_r, i_\alpha] \quad (4.5)$$

$$T_{d-\alpha}[i_\alpha] = \sum_{i_r=0}^{N_r-1} T_{d-r\alpha}[i_r, i_\alpha] \quad (4.6)$$

To compute the total diffuse reflectance and transmittance, we sum the 1-D arrays:

$$R_d = \sum_{i_r=0}^{N_r-1} R_{d-r}[i_r] \quad (4.7)$$

$$T_d = \sum_{i_r=0}^{N_r-1} T_{d-r}[i_r] \quad (4.8)$$

These arrays provide the total photon weight per grid element based on N initial photon packets with unit weight. To convert the raw $R_{d-r\alpha}[i_r, i_\alpha]$ and $T_{d-r\alpha}[i_r, i_\alpha]$ into photon probability per unit area perpendicular to the photon direction per solid angle, they are divided by the projection of the annular area onto a plane perpendicular to the photon exiting direction ($\Delta a \cos \alpha$), the solid angle ($\Delta \Omega$) spanned by a grid separation in the α direction around an annular ring, and the total number of photon packets (N):

$$R_{d-r\alpha}[i_r, i_\alpha] \leftarrow R_{d-r\alpha}[i_r, i_\alpha] / (\Delta a \cos \alpha \Delta \Omega N) [\text{cm}^{-2} \text{sr}^{-1}] \quad (4.9)$$

$$T_{d-r\alpha}[i_r, i_\alpha] \leftarrow T_{d-r\alpha}[i_r, i_\alpha] / (\Delta a \cos \alpha \Delta \Omega N) [\text{cm}^{-2} \text{sr}^{-1}] \quad (4.10)$$

where

$$\Delta a = 2\pi(i_r + 0.5)(\Delta r)^2 [\text{cm}^2] \quad (4.11)$$

$$\Delta \Omega = 4\pi \sin[(i_\alpha + 0.5)\Delta\alpha] \sin(\Delta\alpha/2) [\text{sr}] \quad (4.12)$$

where r and α are computed from Eq. 4.1 and Eq. 4.2, respectively. The raw, radially resolved diffuse reflectance $R_{d-r}[i_r]$ and diffuse transmittance $T_{d-r}[i_r]$ are divided by the area of the annular ring (Δa) and the total number of photon packets (N) to convert them into photon probability per unit area:

$$R_{d-r}[i_r] \leftarrow R_{d-r}[i_r]/(\Delta a N) [\text{cm}^{-2}] \quad (4.13)$$

$$T_{d-r}[i_r] \leftarrow T_{d-r}[i_r]/(\Delta a N) [\text{cm}^{-2}] \quad (4.14)$$

The raw $R_{d-r}[-1]$ and $T_{d-r}[-1]$ need only to be normalized by N to get total unscattered reflectance and transmittance, respectively. Then $R_{d-r}[-1]$ is augmented by the specular reflectance R_{sp} . The raw angularly resolved diffuse reflectance $R_{d-\alpha}[i_\alpha]$ and diffuse transmittance $T_{d-\alpha}[i_\alpha]$ are divided by the solid angle ($\Delta \Omega$) and the total number of photon packets (N) in order to convert them into photon probability per unit solid angle:

$$R_{d-\alpha}[i_\alpha] \leftarrow R_{d-\alpha}[i_\alpha]/(\Delta \Omega N) [\text{sr}^{-1}] \quad (4.15)$$

$$T_{d-\alpha}[i_\alpha] \leftarrow T_{d-\alpha}[i_\alpha]/(\Delta \Omega N) [\text{sr}^{-1}] \quad (4.16)$$

The raw total diffuse reflectance R_d and transmittance T_d are divided by the total number of photon packets (N) to get the probabilities, respectively:

$$R_d \leftarrow R_d/N [-] \quad (4.17)$$

$$T_d \leftarrow T_d/N [-] \quad (4.18)$$

where $[-]$ means dimensionless units.

4.2. Internal photon distribution

During the simulation, the absorbed photon weight is scored into the absorption array $A_{rz}[i_r, i_z]$, where i_r and i_z are the indices for grid elements in r and z directions ($0 \leq i_r \leq N_r - 1$, $0 \leq i_z \leq N_z - 1$ for multiple interactions). $A_{rz}[-1, i_z]$ is used to score the first interactions. The coordinate for each index i_r is shown in Eq.

4.1. The coordinate for each index i_z is the center of a grid element in the z direction:

$$z = (i_z + 0.5) \Delta z \quad (4.19)$$

The raw $A_{rz}[i_r, i_z]$ provides total photon weight in each grid element in the two-dimensional grid system. To get the total photon weight in each grid element in the z direction, we sum the 2-D array in the r direction:

$$A_z[i_z] = \sum_{i_r=0}^{N_r-1} A_{rz}[i_r, i_z] \quad (4.20)$$

The total photon weight absorbed in each layer, $A_l[\text{layer}]$, and the total photon weight absorbed in the tissue, A , can be computed from $A_z[i_z]$:

$$A_l[\text{layer}] = \sum_{i_z \text{ in layer}} A_z[i_z] \quad (4.21)$$

$$A = \sum_{i_z=0}^{N_z-1} A_z[i_z] \quad (4.22)$$

where the summation range ' i_z in layer' includes all i_z values that lead to a z coordinate in the layer. Then, these raw quantities are scaled appropriately to get the densities:

$$A_{rz}[i_r, i_z] \leftarrow A_{rz}[i_r, i_z]/(\Delta a \Delta z N) [\text{cm}^{-3}] \quad (4.23)$$

$$A_{rz}[-1, i_z] \leftarrow A_{rz}[-1, i_z]/(\Delta z N) [\text{cm}^{-3}] \quad (4.24)$$

$$A_z[i_z] \leftarrow A_z[i_z]/(\Delta z N) [\text{cm}^{-1}] \quad (4.25)$$

$$A_l[\text{layer}] \leftarrow A_l[\text{layer}]/N [-] \quad (4.26)$$

$$A \leftarrow A/N [-] \quad (4.27)$$

where Δa is given in Eq. 4.11. The quantity A provides the photon probability of being absorbed by the tissue; the 1-D array $A_l[\text{layer}]$ provides the photon probability of being absorbed in each layer; the array $A_{rz}[i_r, i_z]$ provides the absorption photon probability density (cm^{-3}), which can be converted into photon fluence (cm^{-2}), ϕ_{rz} , by

dividing it by the local absorption coefficient, μ_a (cm^{-1}), of the layer:

$$\phi_{rz}[i_r, i_z] = A_{rz}[i_r, i_z]/\mu_a [\text{cm}^{-2}] \quad (4.28)$$

The 1-D array $A_z[i_z]$ provides the photon probability per unit length in the z direction (cm^{-1}) which can also be divided by the local absorption coefficient, μ_a (cm^{-1}), to yield a dimensionless quantity $\phi_z[i_z]$:

$$\phi_z[i_z] = A_z[i_z]/\mu_a [-] \quad (4.29)$$

At first glance, this quantity may seem difficult to understand, or seem to be redundant. However, the summation of the raw data in Eq. 4.20 equals the convolution for an infinitely wide flat beam [14], which yields the internal fluence as a function of z . For a photon beam that is much wider than the mean free path, the internal fluence at the z -axis as a function of z can be approximated by Eq. 4.29.

The equivalence of Eq. 4.29 to the convolution for an infinitely wide flat beam can be shown as follows. According to Eqs. 4.20, 4.23 and 4.25, the final converted $A_z[i_z]$ and $A_{rz}[i_r, i_z]$ have the following relation:

$$A_z[i_z] = \sum_{i_r=0}^{N_r-1} A_{rz}[i_r, i_z] \Delta a(i_r) \quad (4.30)$$

where $\Delta a(i_r)$ is computed in Eq. 4.11, but here we stress that it is a function of i_r . Employing Eqs. 4.28 and 4.29, Eq. 4.30 can be converted to:

$$\phi_z[i_z] = \sum_{i_r=0}^{N_r-1} \phi_{rz}[i_r, i_z] \Delta a(i_r) \quad (4.31)$$

This is a numerical solution of the following integral:

$$\phi_z(z) = \int_0^\infty \phi_{rz}(r, z) 2\pi r dr \quad (4.32)$$

Eq. 4.32 is the convolution for an infinitely wide flat beam with a unit power density [14]. Therefore, $\phi_z[i_z]$ provides the fluence for an infinitely wide flat beam with a unit power density.

5. Sample computation

Some computational results are described in this section as examples. To verify the program, we compared some of the results with the results from other theories or with the Monte Carlo simulation results from other investigators (detailed results can be found in Ref. 14).

5.1. Total diffuse reflectance and total transmittance

We computed the total diffuse reflectance R_d and total transmittance T_t (including unscattered transmittance) of a slab of turbid medium with the following optical properties: relative refractive index $n = 1$ (i.e. refractive-index-matched boundary), absorption coefficient $\mu_a = 10 \text{ cm}^{-1}$, scattering coefficient $\mu_s = 90 \text{ cm}^{-1}$, anisotropy factor $g = 0.75$, and thickness $d = 0.02 \text{ cm}$. Ten Monte Carlo simulations of 50 000 photon packets each were completed. Then, the averages and the standard errors of the total diffuse reflectance and total transmittance were computed (Table 1). The table also lists the results from van de Hulst's table [28] and from Monte Carlo simulations by Prah et al. [2]. All results agree. The columns ' R_d average' and ' R_d error' are the average and standard error of the total diffuse reflectance, respectively, while the columns ' T_t average' and ' T_t error' are the average and the standard error of the total transmittance.

For a semi-infinite turbid medium that has a mismatched refractive index with the ambient me-

Table 1
Verification of the total diffuse reflectance and the total transmittance in a slab with a refractive-index-matched boundary by comparing with the results from van de Hulst's table [28] and from Monte Carlo simulations by Prah et al. [2]

Source	R_d average	R_d error	T_t average	T_t error
van de Hulst, 1980	0.09739		0.66096	
MCML	0.09734	0.00035	0.66096	0.00020
Prah et al., 1989	0.09711	0.00033	0.66159	0.00049

Table 2

Verification of the total diffuse reflectance in a semi-infinite medium with a refractive-index-mismatched boundary by comparing with the results by Giovanelli [29] and Prah et al. [2]

Source	R_d average	R_d error
Giovanelli, 1955	0.2600	
MCML	0.25907	0.00170
Prah et al., 1989	0.26079	0.00079

dium, the average and the standard error of the total diffuse reflectance are computed similarly and are compared in Table 2 with Giovanelli's [29] results and Monte Carlo simulation results by Prah et al. [2]. The medium has the following optical properties: relative refractive index $n = 1.5$, $\mu_a = 10 \text{ cm}^{-1}$, $\mu_s = 90 \text{ cm}^{-1}$, $g = 0$ (isotropic scattering). Ten Monte Carlo simulations of 5000 photon packets each are completed to compute the average and the standard error of the total diffuse reflectance.

5.2. Angularly resolved diffuse reflectance and transmittance

We used MCML to compute the angularly resolved diffuse reflectance and transmittance of a slab of turbid medium with the following optical properties: relative refractive index $n = 1$, $\mu_a = 10 \text{ cm}^{-1}$, $\mu_s = 90 \text{ cm}^{-1}$, $g = 0.75$, and thickness $d = 0.02 \text{ cm}$. In the simulation, 500 000 photon packets were used, and the number of angular grid elements was 30. The results are compared with the data from van de Hulst's table [28], as shown in Fig. 3.

The variance in Fig. 3a for diffuse reflectance is larger than that in Fig. 3b for diffuse transmittance, which is due to the difference in value between the total diffuse reflectance and the total diffuse transmittance. As shown in Table 1, the total diffuse reflectance is 0.09739, and the total transmittance is 0.66096. Because the unscattered transmittance is $\exp(-(\mu_a + \mu_s)d) = \exp(-2) \approx 0.13534$, the total diffuse transmittance is $0.66096 - 0.13534 = 0.52562$; hence, the total diffuse reflectance (0.09739) is much less than the total diffuse transmittance (0.52562).

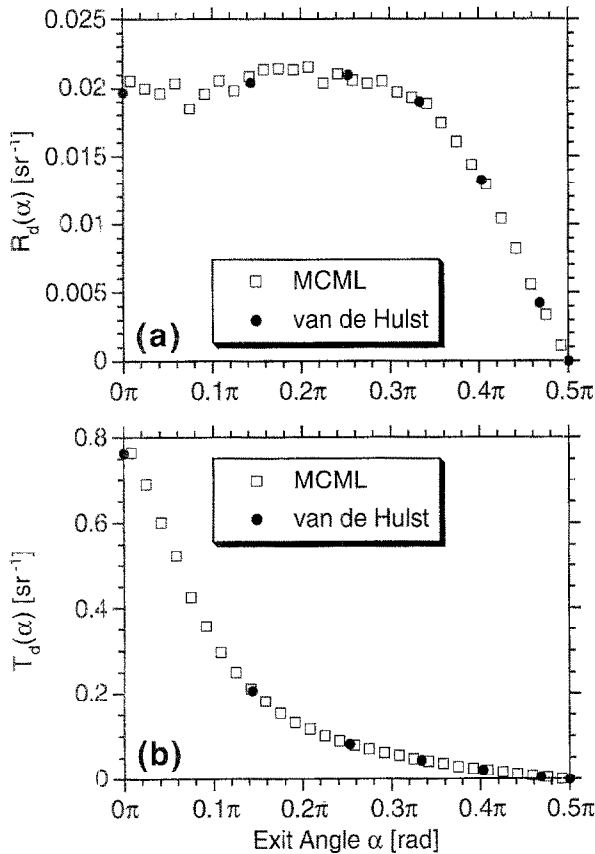


Fig. 3. Angularly resolved (a) diffuse reflectance $R_d(\alpha)$ and (b) diffuse transmittance $T_d(\alpha)$ vs. the angle α , where α is the angle between the photon exiting direction and the normal to the medium surface. Solid circles are from van de Hulst's table and open square boxes are from MCML simulation. The optical parameters are: relative refractive index $n = 1.0$, $\mu_a = 10 \text{ cm}^{-1}$, $\mu_s = 90 \text{ cm}^{-1}$, $g = 0$, thickness $d = 0.02 \text{ cm}$.

Because van de Hulst [28] used a different definition of reflectance and transmittance of exiting angles than we did, and a normalization to incident flux π , we multiplied van de Hulst's data by the cosine of the exiting angle from the normal to the surface, then divided by π .

5.3. Depth resolved internal fluence

As an example, we show the depth resolved internal fluences for two semi-infinite media with refractive-index-matched and refractive-index-mismatched boundaries, respectively (Fig. 4). The dimensionless internal fluence as a function of depth z , $\phi_z[i_z]$, described in Section 4.2 is com-

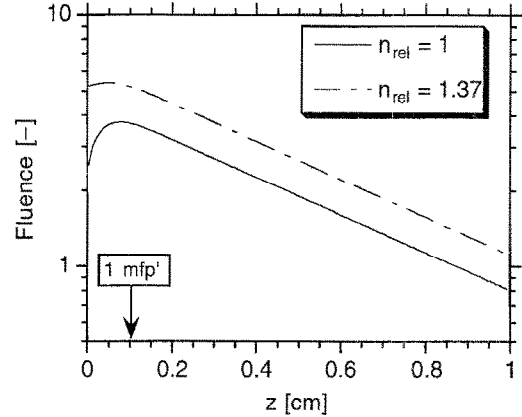


Fig. 4. Comparison of internal fluences as a function of depth z for two semi-infinite media with a refractive-index-matched boundary and a refractive-index-mismatched boundary, respectively. The optical parameters are: relative refractive index $n = 1.0$ or 1.37 , $\mu_a = 0.1 \text{ cm}^{-1}$, $\mu_s = 100 \text{ cm}^{-1}$, $g = 0.9$. The results are from Monte Carlo simulations with 1 million photon packets, each using MCML. The grid line separation and number of grid elements in the z direction are 0.005 cm and 200 , respectively.

puted from the impulse response to an infinitely narrow photon beam, normally incident on a semi-infinite medium. However, it can be equivalently considered as the response of an infinitely wide photon beam with a unit power density perpendicularly incident on a semi-infinite medium (see Section 4.2). Because the direct output of the program MCML provides $A_z[i_z]$ instead of $\phi_z[i_z]$, we divided $A_z[i_z]$ by the absorption coefficient of the semi-infinite medium to obtain $\phi_z[i_z]$. Although the impulse response is considered (Fig. 4), if the input photon beam is measured in W/cm^2 or J/cm^2 as the power density or energy density, the unit of fluence is also in the unit of W/cm^2 or J/cm^2 , correspondingly. Because we consider only steady-state responses, we can discuss either energy density or power density because they can be converted back and forth.

The fluence near the surface is larger than one because the back scattered light augments the fluence. Furthermore, the internal fluence for the medium with a refractive-index-mismatched boundary is higher than that for the medium with a refractive-index-matched boundary. This is due to the internal reflection by the refractive-index-mismatched boundary, therefore, the photons that

would escape from the refractive-index-matched boundary of a medium may be reflected back into the medium by the refractive-index-mismatched boundary and, hence, have an increased chance to be absorbed. When z is sufficiently deep, the two curves are parallel, which confirms the valid range of diffusion theory. For z larger than the penetration depth δ , diffusion theory [30] predicts that the internal fluence distribution should be:

$$\phi(z) = \phi_0 k \exp(-z/\delta) \quad (5.1)$$

where k is a scalar that depends on the amount of back scattered reflectance, and ϕ_0 is the incident irradiance, which is one in our MCML simulation. The scalar k is obviously a function of the relative index of refraction. Therefore, the refractive-index-matched boundary and the refractive-index-mismatched boundary will have different k values. The penetration depth δ is computed:

$$\begin{aligned} \delta &= 1/\sqrt{3\mu_a(\mu_a + \mu_s(1 - g))} \\ &= 1/\sqrt{3(0.1)(0.1 + 100(1 - 0.9))} \approx 0.57 \text{ cm} \end{aligned} \quad (5.2)$$

which is independent of relative index of refraction. Therefore, the two curves in Fig. 4 should be off by just one factor due to different k values when $z > \delta$, which means the curves are parallel in a log-linear plot when $z > \delta$. The two curves shown here are parallel even when $z > 1 \text{ mfp}' = 1/(\mu_a + \mu_s(1 - g)) \approx 0.1 \text{ cm}$, where mfp' is the transport mean free path. One mfp' may be a better criterion for valid application of diffusion theory than the penetration depth δ . Further supporting evidence can be found in Ref. 31.

We fit the parallel part of the two curves with exponential functions. The damping constants for the curves are approximately 1.73 cm^{-1} for the refractive-index matched boundary and 1.74 cm^{-1} for the refractive-index-mismatched boundary. The reciprocals of the damping constants are 0.578 cm for the refractive-index-matched boundary and 0.575 cm for the refractive-index-mismatched boundary. They are very close to the penetration depth (0.57 cm , Eq. 5.2) predicted from diffusion theory.

6. Summary

A Monte Carlo model of steady-state light transport in multi-layered tissues (MCML) has been coded in ANSI Standard C. As a result, the program can be executed on various computers as long as they support ANSI Standard C. We have successfully tested MCML on IBM PC/compatibles, Macintoshes, Sun SPARCstations 2, SiliconGraphics IRIS workstations, and IBM RISC/6000 POWERstations 320. Also, we have verified some of the MCML computational results with those of other theories or other investigators. We have been developing a more general Monte Carlo code to simulate light transport in composite turbid media which can include complex geometric shapes. [32]

Dynamic data allocation is used for MCML, hence the number of tissue layers and grid elements of the grid system can be varied by users at run time provided that the total amount of memory needed does not exceed what the system allocates. Therefore, this method of data allocation is more flexible than defining static arrays of fixed size at compile time.

In MCML, photon pathlength in clear layers does not contribute to the sampled optical pathlength for an interaction with tissue to occur. Hence, no photons will be absorbed by the clear media, which was expected.

Instead of using the centers of grid elements, the coordinates of the simulated data for each grid element in the radial and angular directions are optimized. The deviation of the center from the optimized point in the first grid element is 25% and decreases as the index to the grid element increases. Because the optimized coordinates are computed only after simulating the photons, the optimized coordinates do not increase the simulation time to allow better precision. More importantly, we learned to consider the linearity rather than the resolution in grid elements because to achieve improved resolution we can interpolate the data. Therefore, we select the maximum grid size while satisfying linearity of grid elements in order to reduce the statistical variance in the Monte Carlo simulations.

The Monte Carlo simulation package can be downloaded from our anonymous FTP site (host

name: laser.mda.uth.tmc.edu, I.P. address: 129.106.60.92) or obtained from the authors (Email: lihong@laser.mda.uth.tmc.edu).

Acknowledgments

We thank Marleen Keijzer for providing her Monte Carlo simulation program in PASCAL on Macintosh computers, and Dana Evans for proofreading the manuscript. This research was supported in part by the Whitaker Foundation, the Office of Naval Research N00014-91-J-1354, the Air Force Office of Scientific Research F49620-93-1-0298DEF, the National Institutes of Health R29-HL45045.

References

- [1] B.C. Wilson and G. Adam, A Monte Carlo Model for the absorption and flux distributions of light in tissue, *Med. Phys.* 10 (1983) 824–830.
- [2] S.A. Prah, M. Keijzer, S.L. Jacques and A.J. Welch, A Monte Carlo model of light propagation in tissue, *Proc. SPIE IS 5* (1989) 102–111.
- [3] M. Keijzer, S.L. Jacques, S.A. Prah and A.J. Welch, Light distributions in artery tissue: Monte Carlo simulations for finite-diameter laser beams, *Lasers Surg. Med.* 9 (1989) 148–154.
- [4] S.T. Flock, B.C. Wilson, D.R. Wyman and M.S. Patterson, Monte-Carlo modeling of light-propagation in highly scattering tissues — I: model predictions and comparison with diffusion theory, *IEEE Trans. Biomed. Eng.* 36 (1989) 1162–1168.
- [5] S.T. Flock, B.C. Wilson and M.S. Patterson, Monte Carlo modeling of light propagation in highly scattering tissues — II: comparison with measurements in phantoms, *IEEE Trans. Biomed. Eng.* 36 (1989) 1169–1173.
- [6] M. Keijzer, J.W. Pickering and M.J.C. van Gemert, Laser beam diameter for port wine stain treatment, *Lasers Surg. Med.* 11 (1991) 601–605.
- [7] S.L. Jacques and L.-H. Wang, Monte Carlo modeling of light transport in tissues, in: *Optical Thermal Response of Laser Irradiated Tissue*, Eds. A.J. Welch and M.J.C. van Gemert, in press (Plenum Press, 1995).
- [8] I. Lux and L. Koblinger, *Monte Carlo Particle Transport Methods: Neutron and Photon Calculations* (CRC Press, Boca Raton, FL, 1991).
- [9] W.F. Cheong, S.A. Prah and A.J. Welch, A review of the optical properties of biological tissues, *IEEE J. Quantum Electron.* 26 (1990) 2166–2185.
- [10] L.G. Henyey and J.L. Greenstein, Diffuse radiation in the galaxy, *Astrophys. J.* 93 (1941) 70–83.
- [11] C.M. Gardner and A.J. Welch, Monte Carlo simulation of light transport in tissue: unscattered absorption events, *Appl. Opt.* 33 (1994) 2743–2745.
- [12] E.D. Cashwell and C.J. Everett, *A Practical Manual on the Monte Carlo Method for Random Walk Problems* (Pergamon Press, New York, 1959).
- [13] M.H. Kalos and P.A. Whitlock, *Monte Carlo Methods, I: Basics* (John Wiley & Sons, Inc., 1986).
- [14] L.-H. Wang and S.L. Jacques, *Monte Carlo Modeling of Light Transport in Multi-layered Tissues in Standard C* (University of Texas M.D. Anderson Cancer Center, 1992).
- [15] H. Kahn and T.E. Harris, Estimation of particle transmission by random sampling Monte Carlo method, in: *National Bureau of Standards Applied Mathematics Series No. 12* (U.S. Government Printing Office, 1951).
- [16] A. Ishimaru, *Wave Propagation and Scattering in Random Media* (Academic Press, New York, 1978).
- [17] M. Born and E. Wolf, *Principles of Optics: Electromagnetic Theory of Propagation, Interference and Diffraction of Light*, 6th edn. (corrected) (Pergamon Press, 1986).
- [18] E. Hecht, *Optics*, 2nd edn. (Addison & Wesley Publishing Company, Inc. 1987).
- [19] J.H. Ahrens and U. Dieter, Computer methods for sampling for the exponential and normal distributions, *Comm. ACM* 15 (1972) 873–882.
- [20] G. Marsaglia, Generating exponential random variables, *Ann. Math. Stat.* 32 (1961) 899–900.
- [21] M.D. MacLaren, G. Marsaglia and T. Bray, A fast procedure for generating exponential random variables, *Comm. ACM* 7 (1964) 298–300.
- [22] S.L. Jacques, C.A. Alter and S.A. Prah, Angular dependence of HeNe laser light scattering by human dermis, *Lasers Life Sci.* 1 (1987) 309–333.
- [23] P.J. Plauger and J. Brodie, *Standard C* (Microsoft Press, 1989).
- [24] J.S. Hendricks and T.E. Booth, MCNP variance reduction overview, *Lect. Notes Phys.* 240 (1985) 83–92.
- [25] L.L. Carter and E.D. Cashwell, *Particle-Transport Simulation with the Monte Carlo Method* (USERDA Technical Information Center, Oak Ridge, TN, 1975).
- [26] W.H. Press, B.P. Flannery, S.A. Teukolsky and W.T. Vetterling, *Numerical Recipes in C* (Cambridge Univ. Press, 1988).
- [27] L.-H. Wang and S.L. Jacques, Optimized radial and angular positions in Monte Carlo modeling, *Med. Phys.* 21 (1994) 1081–1083.
- [28] H.C. van de Hulst, *Multiple Light Scattering*, Vol. II (Academic Press, New York, 1980).
- [29] R.G. Giovanelli, Reflection by semi-infinite diffusers, *Opt. Acta* 2 (1955) 153–162.
- [30] B.C. Wilson and S.L. Jacques, Optical reflectance and transmittance of tissues: principles and applications, *IEEE J. Quantum Electron.* 26 (1990) 2186–2199.
- [31] L.-H. Wang and S.L. Jacques, Hybrid model of Monte Carlo simulation diffusion theory for light reflectance by turbid media, *J. Opt. Soc. Am. A* 10 (1993) 1746–1752.
- [32] L.-H. Wang and S.L. Jacques, Animated simulation of light transport in tissues, *Proc. SPIE*, 2134A (1994) 247–254.